---

**Article:**
Mullis, AM, Jegede, OE, Bigg, TD et al. (2020) Dynamics of core–shell particle formation in drop-tube processed metastable monotectic alloys. Acta Materialia, 188. pp. 591-598. ISSN: 1359-6454

https://doi.org/10.1016/j.actamat.2020.02.017

---

# Dynamics of Core-Shell Particle Formation in Drop-Tube Processed Metastable Monotectic Alloys

*Andrew M Mullis*†*, Oluwatoyin E. Jegede, Timothy D Bigg and Robert F Cochrane*

School of Chemical & Process Engineering, University of Leeds, Leeds LS2 9JT, UK.

†Corresponding Author: e-mail a.m.mullis@leeds.ac.uk , tel +44-113-343-2568

***Abstract***

We examine the apparent size of the core and shell as a function of cooling rate in core-shell particles of the metastable monotectic alloy Co-50 at.% Cu, finding that the volume fraction of the core systematically increases with cooling rate and hence undercooling. A model for this variation is proposed. A Monte-Carlo simulation is used to correct for sectioning effects allowing the true core:shell volume ratio to be estimated. From this, and the observation of a second, spinodal, episode of liquid phase separation we are able to estimate the undercooling at solidification. This permits a calculation of the time available following liquid phase separation for the migration giving rise to the observed core-shell structure to occur and hence the required Marangoni velocity required to such migration.

Keywords: Monotectic Solidification, Rapid Solidification, Undercooling, Liquid Phase Separation.

## 1. Introduction

Monotectic alloys have recently attracted considerable attention due to their potential ability for the creation of novel engineered composite materials, including amorphous-crystalline [1] and amorphous-amorphous [2] structures. The potential application of such alloys is greatest when they are of the metastable monotectic type, that is when the critical temperature for liquid phase separation (LPS) is below the equilibrium liquidus, such that liquid demixing can only be accessed via the undercooled melt [3]. In such systems buoyancy driven separation in the

crucible is avoided and droplet processing techniques such as gas atomization and drop-tube processing permit access to novel structures including a fine dispersion of one phase in a matrix of the other [4] and core-shell type particles [5]. This latter arises for droplets in free-fall when buoyancy driven convection is absent, allowing Marangoni convection to dominate [6].

Relative to stable monotectic systems, the literature on metastable monotectic systems is sparse owing to the transitional nature of the metastable phase. Metastable liquid phase separation (LPS) has been predicted in binary systems displaying an evenly sloping, flat liquidus line on the equilibrium phase diagram [3]. Such systems include Ag-Pb, Cu-Ta, Co-Cu, Cu-Fe Cu-Cr and Cu-Nb, with such metastable liquid phase separation indeed being observed in a number of these. Cu-Nb has for instance been reported to display metastable LPS at the Cu-20 wt% Nb composition [7], with there being evidence that oxygen impurities can extend this range to 5-35 wt% Nb [8]. Similarly, metastable LPS has been observed in melt spun Cu-Cr in the composition range 15-35 wt% Cr [9], although relatively high cooling rates ($> 10^4$ K $s^{-1}$) were required to achieve this. Moreover, the results could not be reproduced in electromagnetic levitation experiments [10], and consequently the undercooling required for LPS remains undetermined in this system. Conversely, Cu-Fe has been demonstrated to undergo metastable LPS relatively easily, with the critical temperature for liquid demixing potentially being only 20 K below the equilibrium liquidus [11]. Similarly, Co-Cu appears to undergo LPS relatively easily over a wide range (16.0 – 87.2 at.% Co) of compositions [12].

The conditions for the formation of core-shell structures are favoured when immiscible alloys are processed using powder metallurgical techniques such as high pressure gas atomization or drop-tube techniques. Buoyancy driven convection is suppressed by free-fall and the high cooling rates experienced by such droplets establishes a temperature gradient between the surface and centre of the droplet to drive Marangoni flow. However, even for simple binary alloys the physical mechanism operating is controversial, with dispute over which phase forms the core and which the shell. Wang *et al*. [5] have argued that the phase with the lower volume fraction will always form the core, a conclusion that appeared to be borne out by phase-field simulations [13]. However, there are multiple reports of cases that appear to contradict this, including in the Al-Bi system in which Al is reported to always form

the core even when Bi had the lower volume fraction [14]. This has led to an alternate hypothesis that it is the higher surface tension, and hence higher melting point, liquid which forms the core surrounded by a shell of the lower melting point liquid.

The time available for migration of the demixed liquids has also been shown to be a critical factor in determining the extent of core-shell formation. [15] have demonstrated that alloys near their critical composition have a stronger tendency to form core-shell particles, the lower undercooling required to access LPS resulting in a longer migration time prior to solidification of the sample. In a drop-tube study of Co-Cu alloys [16] showed that there is a complex relationship between cooling rate and morphology, with higher cooling rates giving higher undercoolings, which promote LPS, but also shorter migration times. This was shown to result in a wide range of final structures in the as-solidified samples including: fully developed core-shell structures, evolving core-shell structures and a fine uniform dispersion of Co-rich particles in a Cu-rich matrix. Moreover, the likelihood of fully developed core-shell structures was shown to be a non-monotonic function of the particle size, with core-shell formation most likely (> 80% of LPS particles examined) in the 106-75 μm sieve fraction for a Co-50 at.% Cu alloy but in the 150-160 μm sieve fraction for a Co-68.5 at.% Cu alloy. For both compositions the probability of finding fully developed core-shell structures was much lower in both the larger and smaller diameter sieve sizes.

One of the key challenges in the greater application of functionalized core-shell particles is that of obtaining good control over the relative volume fractions of the core and shell. This has been explored extensively with regard to composition [17, 18], but virtually no consideration has been given to the potential dependence of the core/shell volume ratio upon undercooling. In this paper we make a systematic study of the core/shell ratio in Co-50.0 at.% Cu alloy as a function of cooling rate, and hence undercooling, during drop-tube processing.

The metastable phase diagram for the Co-Cu system has been the subject of some debate. Using differential thermal analysis [12] were able to directly measure both the liquidus and LPS temperatures for Co-Cu alloys over the composition range 16.0 – 87.2 at.% Co. They determined the critical composition as 53 at.% Cu, wherein the LPS temperature was determined as 1547 K, 108 K below the equilibrium liquidus temperature. This was 30 K lower

than the previous estimate of the separation temperature by Nakagawa *et al*. [11], while later flux undercooling experiments by [19] placed the LPS temperature 96 K below the liquidus temperature. CALPHAD calculations by Palumbo *et al*. [20] placed the critical composition at 58.5 at.% Cu with a corresponding temperature of 1556 K, an undercooling of around 80 K. Here we have adopted the metastable phase diagram calculated by [16] using the assessed thermodynamic data of [21]. The critical composition is placed at 58.7 at.% Cu, in good agreement with [20], although the separation temperature is somewhat higher at 1623 K, resulting in a somewhat lower minimum undercooling for LPS. The phase diagram, complete with metastable extension for the binode, is shown in **Figure 1**.

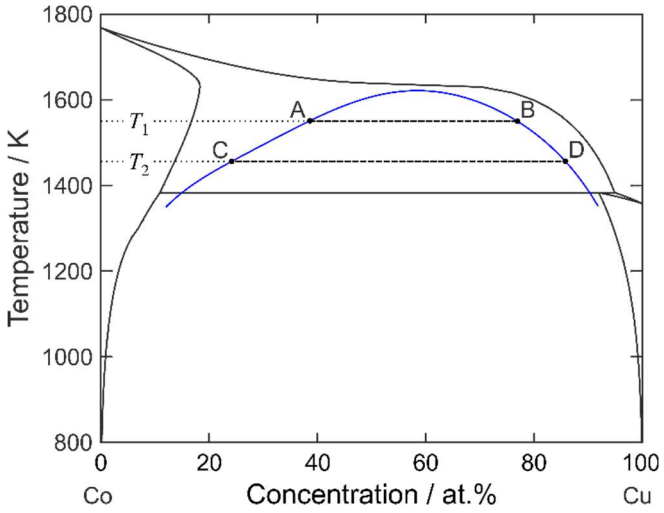


**Figure 1.** Phase diagram for the Co-Cu system including the metastable binode for liquid phase separation. For liquid phase separation nucleated at a temperature $T_1$ the result will be a Co-rich liquid of composition marked by point A and a Cu-rich liquid of composition marked by point B. For the lower temperature, $T_2$, the compositions shift to those marked by points C and D respectively.

## 2. Experimental Methods

High purity Co and Cu (99.99% and 99.999% respectively) were obtained from Alfa Aesar. Ingots of the Co-50 at.% Cu master alloy were produced by arc melting the correct amount of each constituent together under a protective argon atmosphere. The arc furnace utilises a water cooled Cu hearth and tungsten electrode, wherein the material in contact with the hearth

solidifies more rapidly than that in contact with the argon atmosphere near the electrode. Each ingot was arc melted 5 times to ensure complete mixing of the constituents, with the sample being flipped each time so that the surfaces nearest the hearth and electrode were reversed. Following the final melting cycle the microstructure of the ingot was examined. On the hearth side of the ingot we observed a fine dispersion of Co-rich droplets in a Cu-rich matrix while on the atmosphere side we observed Co-rich dendrites in a Cu-rich matrix. This would indicate that liquid phase separation had occurred on the side of the sample in contact with the hearth, but not on the side of the sample nearest the electrode. Notwithstanding this, once sectioned in the transverse direction, i.e. from the hearth- to the electrode-side of the sample, ICP analysis showed that the master alloy for the drop-tube experiments had the correct bulk composition.

Atomization of the melt was achieved using the Leeds 6.5 m drop-tube. A transverse slice of the ingot, of around 7 g in mass, is loaded into an alumina crucible with 3 x 300 μm laser drilled holes in the base. The crucible is then loaded into a graphite sleeve which makes a pressure tight seal at the top of the tube. A turbomolecular pump is used to reduce the pressure in the tube to $10^{-4}$ Pa, before backfilling to 40 kPa with an oxygen free inert gas atmosphere. Melting of the sample is achieved using a 3 kW induction heater, with the graphite sleeve providing good coupling to the RF field. Temperature determination is by means of an R-type thermocouple located inside the crucible, just above the level of the melt. At a melt temperature of 1900 K (≈ 130 K above the Co melting temperature) the crucible is pressurised to 400 kPa, wherein a spray of droplets of various sizes is ejected down the tube. These solidify in flight, with the solid powder being collected at the bottom of the tube.

Once removed from the tube the powders are sieved into standard sizes, using a sieve stack with the following mesh sizes: 850 μm, 500 μm, 300 μm, 212 μm, 150 μm,106 μm, 75 μm, 53 μm and 38 μm. Each size fraction is mounted in Transoptic resin before being ground and polished to a 1 μm finish using diamond paste. Microstructure determination was undertaken utilising both optical microscopy using a Nikon Optiphot microscope, and scanning electron microscopy, using a Carl Zeiss Evo MA15 SEM. For SEM the polished samples were etched for 20 s in a Nital solution (2% nitric acid in propan-2-ol). For optical microscopy no etching was required as there was sufficient colour contrast between the Co- and Cu-rich phases.

Determination of particle cooling rate utilises the model developed in [22] for the balance of heat fluxes, assuming that particles rapidly attain terminal velocity. Full details of the model are given in [22], with the parameters appropriate to the processing of Co-Cu melts in nitrogen being given in [16]. The resulting estimated cooling rate, as a function of droplet size, is shown in **Figure 2**, where the error bars show the level of uncertainty resulting from grouping particles in standard sieve sizes, i.e. in the 212-150 μm sieve fraction the upper limit of the error bar corresponds to the cooling of a 150 μm particle and the lower error bar to that of a 212 μm particle, with the error bar being located at the midpoint of the range, namely 181μm.

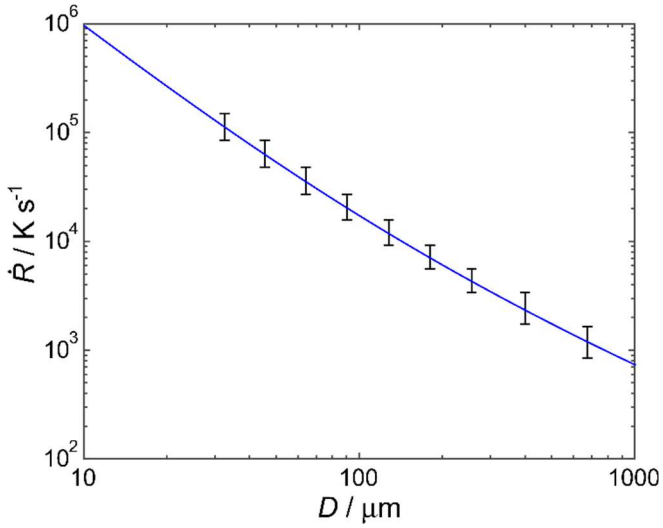


**Figure 2.** Calculated cooling rate for Co-50 at.% Cu alloy drop-tube processed in 40 kPa nitrogen. Error bars denote variability due to classifying particles in standard sieve fractions.

## 3. Results

An example optical micrograph of a core-shell type particle, in this case from the 106-75 μm sieve fraction, is shown in **Figure 3a**. In this case the sample has not been etched, with the colour contrast between the Cu-rich shell and Co-rich core providing sufficient differentiation between the two phases to facilitate measurement of the core diameter. Also evident in the micrograph are Co-rich inclusions within the shell region and Cu-rich inclusions within the core region. A model for the origin of such inclusions has been proposed by [23] and may be

explained with reference to **Figure 1**. We assume that nucleation of binodal decomposition occurs at some temperature, $T_1$, below the liquidus, wherein liquid phase separation occurs to Co-rich and Cu-rich liquids, with compositions denote by points A and B respectively on the phase diagram occurs. In most cases further undercooling of the melt will occur as the migration of the two liquids takes place, potentially resulting in a second episode of liquid phase separation if the temperature drops below the spinode. Consequently, virtually all core-shell particles observed in this system appear to have undergone spinodal decomposition of the Co-rich liquid in the core, giving rise to a distribution of Cu-rich inclusions as evident in **Figure 3a**. However, this is not always the case in the Cu-rich shell, in which we variously observe either spherical Co-rich inclusions or Co-rich dendrites as shown in **Figures 3b & 3c** respectively. This observation is discussed in more detail later.

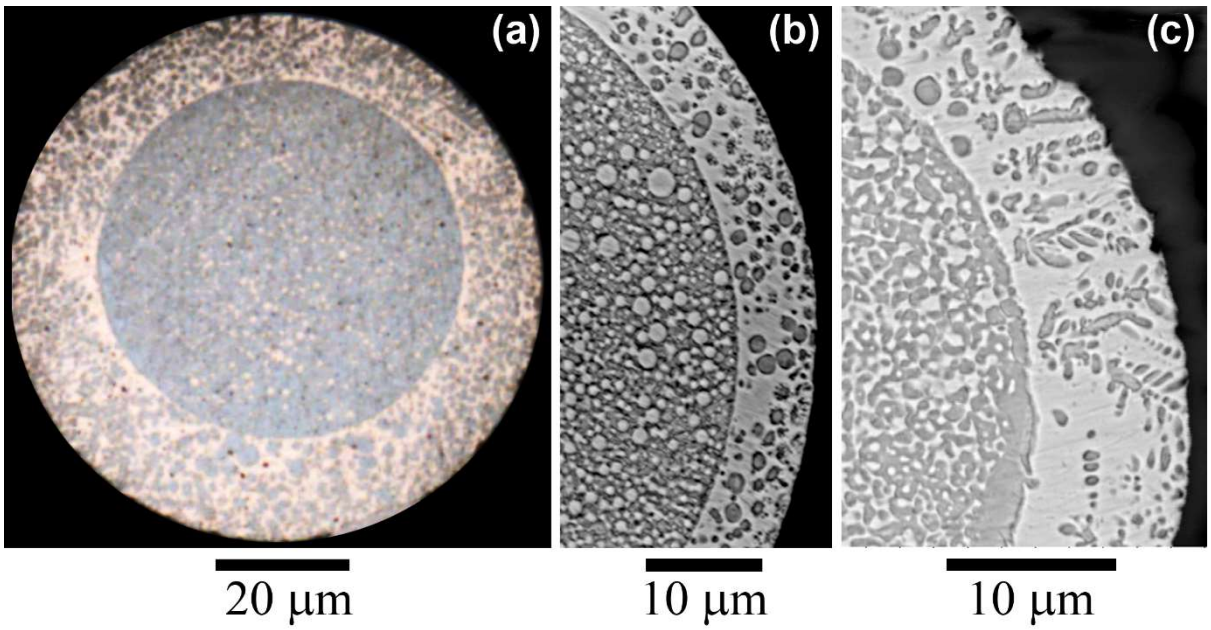


**Figure 3.** (a) Optical micrograph of a particle showing clear delineation of a Co-rich core and Cu-rich shell in an unetched droplet. Note that secondary liquid phase separation gives rise to Co-rich inclusions in the shell and Cu-rich inclusions in the core. (b & C) SEM micrograph of a Cu-rich shell region showing (b) spherical and (c) dendritic Co-rich inclusions (both etched in natal).

As the specific volume of the Co- and Cu-rich phases is very similar, we assume that this second episode of phase separation, whether it be in the liquid phase or upon solidification, does not affect the size ratio of the core to that of the shell. That is, the measured core size, with *as solidified* Cu-rich inclusions, represents the same overall fraction of the droplet as it would have done upon liquid phase separation to a liquid of concentration A. Note that in this regard the bulk composition of the shell, with inclusions, will be identical to that at point A.

The *apparent* shell volume fraction, as a function of sieve size, measured from the assembled core-shell micrographs, is shown in **Figure 4**. It is clear from the plot that as the particle (sieve) size decreases the average *apparent* volume fraction occupied by the shell increases from a minimum value of 19.7% in the 500-300 μm sieve fraction to a maximum value of 55.7% in the 53-38 μm sieve fraction. As the undercooling of drop-tube processed samples will increase with decreasing particle size, due both to the increased cooling rate of such samples and due to the melt sub-division effect, this is equivalent to the volume fraction of the shell increasing with undercooling. As such, the large scatter observed in the data is likely to be a consequence of the stochastic nature of nucleation, with different droplets, even within the same size fraction, attaining potentially very different levels of undercooling.

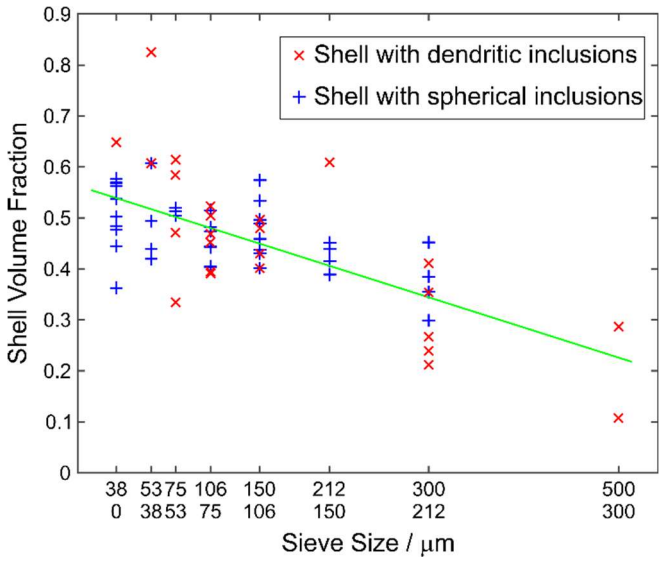


**Figure 4.** *Apparent* shell volume fraction as a function of sieve size in drop-tube processed Co-50 at.% Cu alloy.

As far as we are aware, such a systematic trend has not been reported in other core-shell forming systems, although it may be explained in a relatively straightforward manner with reference to the phase diagram. It is apparent from the phase diagram that as the binodal decomposition temperature decreases the Co-rich liquid becomes more Co-rich (point A moves to the left) and that the Cu-rich liquid becomes more Cu-rich (point B moves to the right). This is shown in **Figure 1** by the point C and D which correspond to the lower LPS temperature, $T_2$. If the binode were symmetric and the alloy composition coincided with the critical composition this would have no effect on the core-shell volume fraction. However, as noted by [16], the binode is not symmetric, being shallower on the Co-rich side than on the Cu-rich side of the phase diagram. Consequently, as the undercooling increases the Co-rich liquid becomes enriched in Co more rapidly than the Cu-rich liquid becomes enriched in Cu. By way of example, at a temperature of 1550 K the concentrations of the Co- and Cu- rich liquids at the binode are 38.4 at.% (40.2 wt%) Cu and 76.9 at.% (78.3 wt%) Cu respectively. At these compositions, $|m|$ is 0.163 at.% $K^{-1}$ (0.165 wt% $K^{-1}$) for the Co-rich liquid but only 0.127 at.% $K^{-1}$ (0.121 wt% $K^{-1}$) for the Cu-rich liquid, with $m$ being the gradient of the liquidus. Applying the Lever rule, it is clear that the consequence of this asymmetry is that the volume fraction of the Cu-rich liquid, and hence of the shell, increases as the undercooling increases.

In principal, the trend observed in **Figure 4**, and the associated relationship with the phase diagram, could lead to an interesting means of determining experimentally the undercooling at which LPS was nucleated in these drop-tube processed samples. There is however a problem. For a randomly distributed microstructure the area estimate of a given phase in cross section is an unbiased estimator of the volume fraction of that phase in the bulk. This is not true for a spherical core-shell structure. Below, we explore how we might account for this geometrical sectioning effect in a statistical manner and hence how the nucleation undercooling for binodal decomposition can be estimated.

## 4. A Model to Estimate Nucleation Undercooling for LPS

As shown in **Figure 5**, for a spherical core-shell particle with true particle diameter $D_t$ and true core diameter $d_t$ sectioning is potentially problematic. Sectioning exactly on the equatorial

plane leads to the apparent diameter for the particle and core being $D_a = D_t$ and $d_a = d_t$, respectively. However, sectioning at any height, $z$, above the equatorial plane reduces both $D_a$ and $d_a$ below their corresponding true values. In order to compensate for this we employ a Monte-Carlo type correction algorithm, in which we use a randomly assigned true particle diameter to estimate $z$ and hence calculate the likely true particle and core diameters.

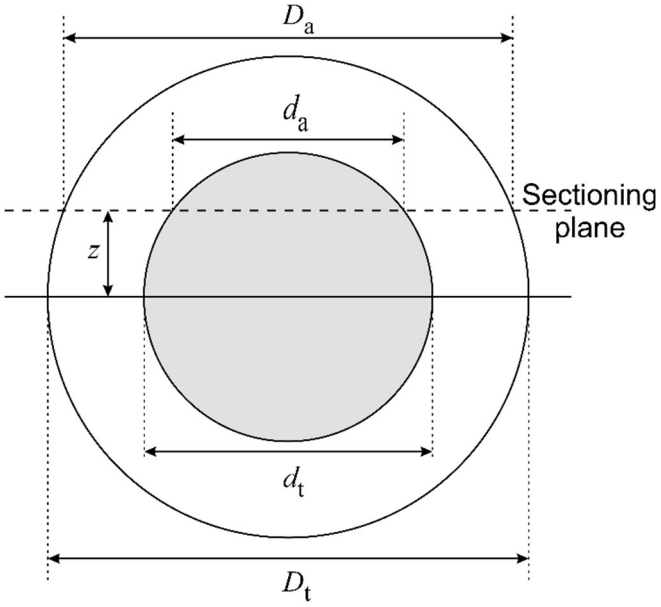


**Figure 5.** Schematic diagram showing the relationship between true and apparent diameter as a function of sectioning height, $z$, above the equatorial plane of a droplet.

For a given sieve fraction the upper and lower limits on the particle diameter will be $D_u$ and $D_l$ respectively, where by convention $D_u/D_l = \sqrt{2}$. Consequently, for a given particle observed in cross section, the true diameter is bounded: $D_u \leq D_t \leq D_a$, i.e. the true particle diameter can be no larger than the maximum size allowed by the sieve and no smaller than its measured apparent diameter. We therefore randomly assign an estimate, $\tilde{D}_t$, of the true diameter such that $D_u \leq \tilde{D}_t \leq D_a$. With an estimate of the true particle diameter, $\tilde{D}_t$, we then use trigonometry to estimate $z$, wherein it is a straightforward matter to work back from $d_a$ to obtain an estimate of the true core diameter $\tilde{d}_t$. This process is then repeated a large number of times (typically $N = 1000$), for different randomly generated values of $\tilde{D}_t$, in order to obtain

a best estimate of the true core diameter, $\hat{d}_t$, for each particle, from which the estimated true core:shell volume ratio may be calculated.

The results of this analysis are shown in **Figure 6**. Comparing **Figure 4** with **Figure 6** it is clear that the effect of the Monte-Carlo correction is to:

1) Reduce the size of the shell volume fraction. This is to be expected as the objective of the routine is to correct for the under estimation of the core diameter in the cross-section due to sectioning out of the equatorial plane.
2) Somewhat reduce the scatter in the data for each size fraction. This appears to be because droplets with the highest *apparent* shell volume (smallest core diameter) also have the smallest *apparent* droplet diameter. There is therefore a larger range, $D_u \leq \tilde{D}_t \leq D_a$, over which the correction can be applied, tending to increase its effect.

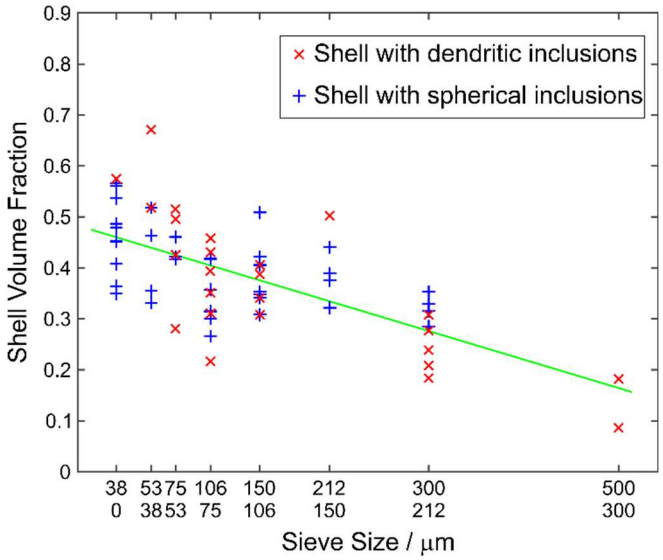


**Figure 6.** Estimated true shell volume fraction as a function of sieve size following application of a Monte-Carlo correction for sectioning height in drop-tube processed Co-50 at.% Cu alloy.

With an estimate of the true shell volume fraction we can then estimate the undercooling at which LPS occurred in the following manner. With reference to **Figure 1** we note that LPS at a temperature of $T_1$ will lead to Co- and Cu- rich liquids with compositions given by the points A and B on the phase diagram respectively. Let these be denoted by $C_A$ and $C_B$ (in at.%)

respectively, with the corresponding mass based compositions being $W_A$ and $W_B$. Applying the Lever rule, the mass fraction of the Cu-rich shell phase, $W_{shell}$, is given by:

$$W_{shell} = \frac{W - W_A}{W_B - W_A} \quad (1)$$

where $W$ is the (mass) concentration of the bulk alloy, i.e. 51.88 wt% (50 at.%) Cu. Given $W_{shell}$, it is relatively straightforward to estimate the shell volume fraction, $V_{shell}$, for which we assume that the density of the Co-Cu mixture can be obtained by linear interpolation between the densities for the Co and Cu end members. The resulting map between shell volume fraction and the undercooling at which binodal decomposition was initiated is shown in **Figure 7**.

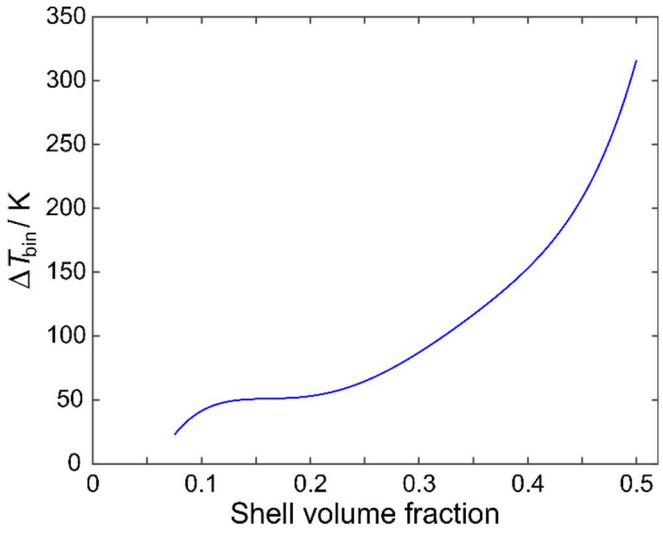


**Figure 7.** Relationship between shell volume fraction and the undercooling at which liquid phase separation by binodal decomposition is initiated.

The resulting estimated undercoolings for each droplet, as a function of droplet size, are shown in **Figure 8**. For most of the droplets in which a core-shell structure was observed it has proved possible to determine an estimated nucleation undercooling for LPS, although in a small number of cases this has not been possible. Generally, this has been for the largest shell volumes, wherein it becomes impossible to obtain a sufficiently large shell mass fraction from Equ. (1) for a 50 at.% Cu alloy. The likelihood is that these instances represent cases in which the droplet has been sectioned a relatively large distance from the equatorial plane (i.e. $z$ large)

and for which the true core diameter is therefore underestimated by the Monte-Carlo correction. Notwithstanding this, we note that there are a number of instances in which the shell volume approaches or exceeds 50% of the estimated true droplet volume. In all such cases we continue to observe a well-developed, Co-rich, core. There is no evidence for an inversion to a Cu-rich core, nor do we observe the absence of core-shell structures in cases where the two phases have the same volume fraction, as would be predicted by the model of [13]. We therefore conclude that the volume fraction of the respective phases has no bearing upon which phase will form the core and which the shell.

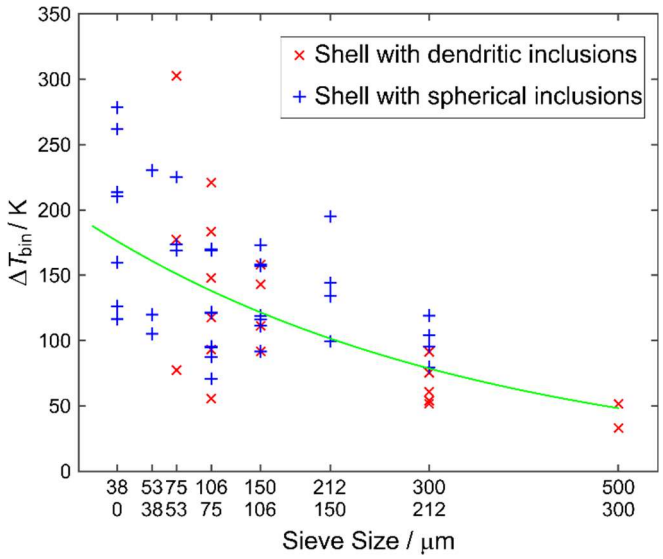


**Figure 8.** Estimated undercooling at binodal decomposition as a function of droplet size for drop-tube processed Co-50 at.% Cu alloy based on the estimated true core:shell volume ratio.

It is also apparent from **Figure 8** that there appears to be little correlation between the estimated LPS temperature and whether the observed structure in the shell is that of spherical or dendritic Co-rich fragments. The structure of these fragments within the shell region is determined by the temperature at solidification, and specifically whether this is above, or below, the temperature required for spinodal decomposition of the Cu-rich liquid. The inference would be that there is little correlation between the undercooling required for nucleation of LPS and the undercooling required for nucleation of solidification. As such, the

finding is consistent with that of [24] who showed that effective nuclei for solidification (e.g. $TiB_2$ grain refiner in Al-based melts) are not necessarily effective nuclei for initiating LPS. Moreover, these observations suggest a route by which a lower bound on the undercooling upon solidification may be estimated, as discussed below.

From the above discussion we have established that, for each particle observed, we can estimate the true core diameter, $\tilde{D}_t$, which in turn leads to estimates of the temperature, and hence undercooling, at which LPS was nucleated and therefore the resulting compositions of the Co-rich and Cu-rich liquids. In the case denoted in **Figure 1** these latter are given by the points A and B for a liquid undergoing binodal decomposition at temperature $T_1$ and the points C and D for binodal decomposition at the lower temperature $T_2$. Now, for the core-shell particles observed, the Co-rich core is always observed to have undergone a second episode of LPS, from which we can deduce that the undercooling corresponding to spinodal decomposition of the Co-rich liquid is invariably achieved prior to nucleation of solidification. Conversely, only some of the droplets also show a second episode of LPS in the Cu-rich shell. This is consistent with the phase diagram of [16], in which the spinodal decomposition temperature is lower on the Cu-rich side of the phase diagram than on the Co-rich side. For those droplets that show a second episode of liquid phase separation in the shell, the lower bound on the undercooling upon nucleation of solidification is given by the spinodal decomposition temperature for the Cu-rich liquid. However, for those droplets that display a dendritic structure in the Cu-rich shell, the corresponding lower bound on the undercooling upon nucleation of solidification would be given by the spinodal decomposition temperature for the Co-rich liquid. Thus with a knowledge of only the core:shell ratio and the microstructure in the shell, a lower bound may be established on the undercooling achieved prior to solidification. The mapping between the core:shell volume ratio and the solidification undercooling is given in **Figure 9**. The lower curve in **Figure 9** (curve A) gives the minimum undercooling for a droplet displaying LPS in the core but a dendritic structure in the shell, whereas the upper curve (curve B) gives the minimum undercooling for a droplet displaying LPS in both core and shell. In both cases the spinodal decomposition temperature as a function of composition is adopted from [16].

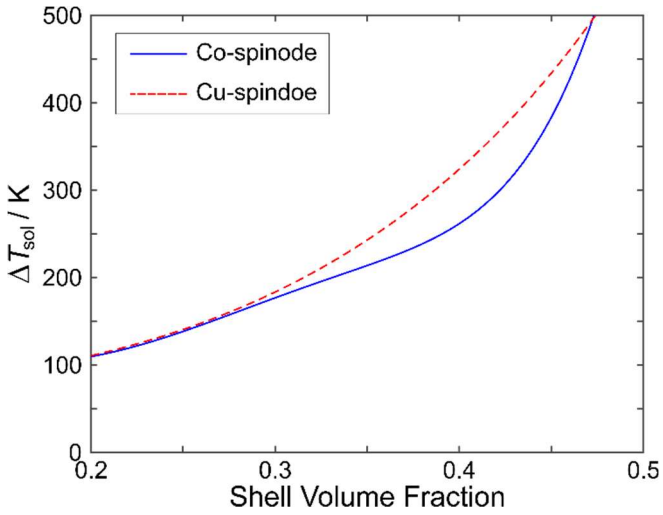


**Figure 9.** Relationship between shell volume fraction and the estimated minimum undercooling at solidification. The Co-spinode is used for samples showing dendritic Co-rich inclusions in the Cu-rich shell, the Cu-spinode for samples showing spherical Co-rich inclusions in the Cu-rich shell.

As such, the procedure for estimating the undercooling at solidification gives a route by which our results may be compared with those of other authors. Using classical nucleation theory Lee & Ahn [25] estimated the solidification undercooling for atomized droplets. This model was subsequently utilised by Wang & Wei [26] to fit the results of their experimental data generated using a drop-tube processing method similar to that employed here. In **Figure 10** we present the mean estimated solidification undercooling for our drop-tube processed Co-Cu alloy as a function of mean particle size, compared with the trend obtained by Wang & Wei. For our experimental data, each data point is the arithmetic mean of the estimated lower bound on the undercooling of all available droplets in that size fraction, while the error bars represent the corresponding standard error. Our estimated lower bound on solidification undercooling range from ≈ 85 K for a 400 μm diameter droplet to nearly 400 K in the < 38 μm sieve fraction. As may be observed, good agreement is obtained with the estimate of Wang & Wei, which is typically 20-30 K higher than our estimate. However, as they estimated the actual undercooling upon nucleation, whereas our estimate is a lower bound on the undercooling, the data appears to be consistent.

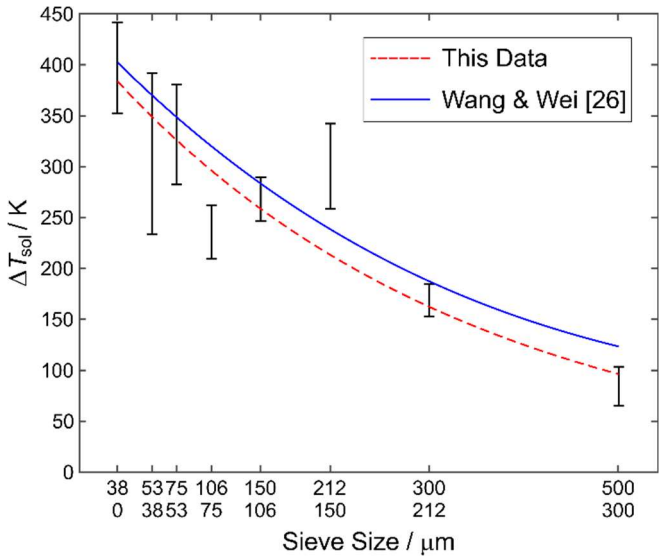


**Figure 10.** Estimated undercooling upon solidification as a function of droplet size for drop-tube processed Co-50 at.% Cu alloy. Also shown, comparison against measured drop-tube undercoolings as determined by Wang and Wei [26].

## 5. Discussion

The mechanics of core-shell formation in liquid phase separated alloys during free-fall is complex. As shown by [16], the likelihood of core-shell formation is a non-monotonic function of droplet size, which is combined, according to the results of this study, with the core:shell volume ratio also depending upon the droplet size, via the undercooling attained whilst in free-fall. The variation in core:shell volume ratio is relatively straightforward to rationalise via the metastable phase diagram. In the case studied here, increased undercooling (smaller droplet size) results in the two liquids becoming more enriched in their majority component, with a similar trend likely to be observed in most other monotectic systems due to the shape of the metastable binode line. However, how this quantitatively effects the core:shell volume ratio will depend critically upon both the nature of the phase diagram and the starting composition of the alloy. With a knowledge of these it should be possible to predict the core:shell volume ratio as a function of undercooling, although for droplet populations produced via techniques such as drop-tube or high pressure gas atomization there will inevitably be some variation in the resulting core:shell volume ratio due to the stochastic nature of nucleation.

Interestingly, the dependence of the core:shell volume ratio upon undercooling also gives us a means to determine the magnitude of the undercoolings achieved by droplets in free-fall. This for instance can be used to calibrate the achievable undercoolings to be expected in drop-tube experiments and as a means of studying nucleation process in small droplets. The undercoolings estimated in our experiments from measurement of core:shell volume ratios appear to be in line with other authors, giving some degree of confidence in the technique. **Figure 11** shows the estimated undercoolings for liquid phase separation and for solidification, now re-plotted as a function of cooling rate. In both cases there is initially a rapid increase in the undercooling achieved with increasing cooling rate, with this levelling off around 5000-7000 K $s^{-1}$. Thereafter, there is a much more gradual increase in achievable undercooling, which is accompanied by a greater degree of scatter. A potential interpretation of this result would be that increasing cooling rate is the dominant mechanism in supressing nucleation for cooling rates up to 5000-7000 K $s^{-1}$. Thereafter, further increases in cooling rate probably have little effect, with the further, slower increase in undercooling being due to an increase in the melt sub-division effect as droplet size decreases.

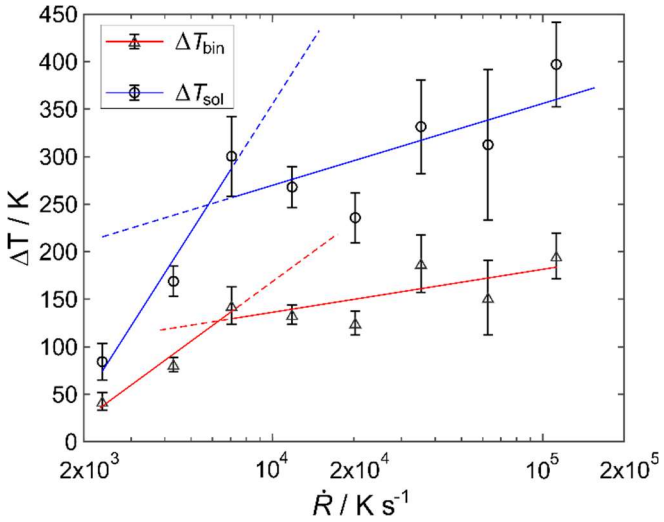


**Figure 11.** Estimated undercooling upon liquid phase separation and upon solidification as a function of cooling rate for drop-tube processed Co-50 at.% Cu alloy.

We return finally to the mechanics of core-shell particle formation and the trend observed by [16], in which the probability of observing a fully formed core-shell structure was a non-monotonic function of droplet size. The formation of core-shell particles depends critically upon droplet size. Small droplets will attain high undercooling, favouring liquid phase separation, but will also cool more rapidly, limiting the time available for migration of the separated liquids. In principle, as we can estimate the undercoolings for both LPS and solidification, the time available for migration can be estimated as a function of droplet size by virtue of the cooling rate being known. Moreover, the distance over which migration needs to occur in order to form a core-shell particle is fixed by the droplet size. Consequently, the minimum Marangoni velocity required for core-shell formation may also be estimated. Both the time available and the consequent minimum Maragoni velocity are shown in **Figure 12**. As shown in the figure, the time available for migration peaks at around 30 ms in the 212-150 μm sieve fraction, wherein a minimum Marangoni velocity of around 3 mm $s^{-1}$ would be required for core-shell formation. This compares with calculated Marangoni velocities of 4-30 mm $s^{-1}$ determined by Wang *et al*. [15]. For larger particles, despite the cooling rate being lower, the difference in undercooling between LPS and solidification decreases, giving rise to a lower overall time available for core-shell formation and a higher required Marangoni velocity. The peak value in the required velocity occurs in the 500-300 μm sieve fraction at a value of 10 mm $s^{-1}$, although this is still comfortably within the range calculated by Wang *et al*. [15]. Conversely, as the particle size is decreased below 212-150 μm the cooling rate is increasing rapidly such that the time available for core-shell formation drops significantly. This leads to an increase in the required minimum Marangoni velocity for complete core migration, with a peak velocity of around 6.5 mm $s^{-1}$ being required for 38 μm droplets.

The trend uncovered here ties in well with the data of [16], who observed that the frequency with which fully developed core-shell structures occur is a non-monotonic function of particle size. They observed that the peak occurrence of such fully developed core-shell structures occurred in the 106-75 μm sieve fraction, with the shift towards smaller sieve fractions likely to be a consequence of the higher probability of LPS in these smaller particles. They observed LPS to be almost twice as likely in the 106-75 μm sieve fraction as in the 212-

150 μm sieve fraction identified here as offering the easiest migration towards a fully developed core-shell structure, with the analysis here being restricted to include only those particles that were observed to have undergone LPS.

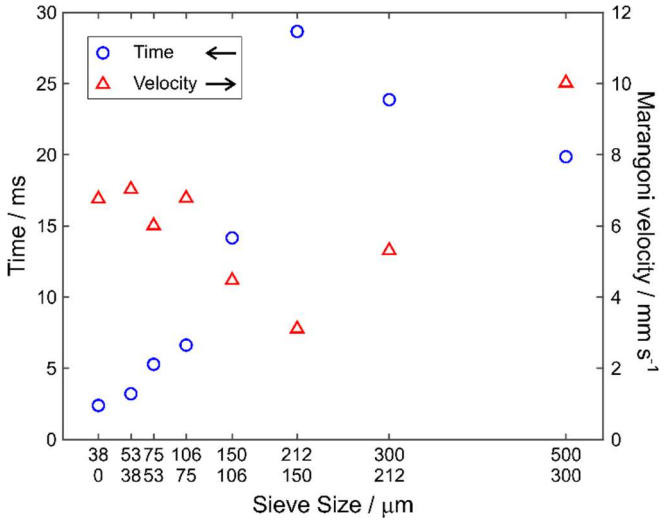


**Figure 12.** (Left-hand axis) Time available for liquid migration to form a core-shell structure based upon the estimated undercoolings for liquid phase separation and for solidifiction, combined with the estimated cooling rate. (Right-hand axis) Corresponding minimum Marangoni velocity required to achieve core-shell formation.

## 6. Summary

We have conducted systematic measurements of the core:shell volume ratio in a sample of Co-50 at.% Cu drop-tube processed alloy droplets, preselected such that all particles display a well-developed core-shell morphology. We find that the apparent volume fraction occupied by the shell increases with decreasing particle size. By applying a Monte-Carlo correction for the sectioning height a true core:shell volume ratio may be estimated, allowing the undercooling at which liquid phase separation occurred to be estimated from the metastable phase diagram. Moreover, the observation of a second (spinodal) decomposition in the core of all samples and the shell of only some samples also allows the undercooling at solidification to be estimated. As a consequence, the time available for migration of the demixed liquids in to a well-developed core-shell structure may be estimated directly from the experimental data, together

with an estimate of the minimum Marangoni velocity required to facilitate the formation of the core-shell structure. We believe that this may provide important data for the validation of models of core-shell particle formation. As an aside, the data relating to the undercooling achieved by particles in free-fall prior to solidification may also be used to estimate the undercoolings achieved by such droplets, as a function of particle size, during powder production techniques such as drop-tube processing and gas atomization.

**Acknowledgements**

This work was funded by MAPP – The EPSRC Future Manufacturing Hub in Manufacture using Advanced Powder Process (Grant No. EP/P006566/1). Oluwatoyin Jegede is a commonwealth scholar, sponsored by the UK government.

**References**

[1] J. He, H.X. Jiang, S. Chen, J.Z. Zhao, L. Zhao: Liquid phase separation in immiscible Ag-Ni-Nb alloy and formation of crystalline/amorphous composite, *J. Non-crystalline Solids* **357** (2011) 3561–3564.

[2] A. Concustell, N. Mattern, H. Wendrock, U. Kuehn, A. Gebert, J. Eckert, A.L. Greer, J. Sort, M.D. Baro: Mechanical properties of a two-phase amorphous Ni-Nb-Y alloy studied by nanoindentation, *Scripta Mater*. **56** (2007) 85–88.

[3] M.B. Robinson, D. Li, T.J. Rathz, G. Williams: Undercooling, liquid separation and solidification of Cu-Co alloys, *J. Mater. Sci.* **34** (1999) 3747–3753.

[4] J.L. Fihey, P. Nguyen-Duy, R. Roberge: On the solidification microstructure of copper-rich niobium alloys, *J. Mater. Sci.* **11** (1976) 2307–2311.

[5] N. Wang, L. Zhang, Y.P. Zheng, W.J. Yao: Shell phase selection and layer numbers of core-shell structure in monotectic alloys with stable miscibility gap, *J. Alloys Compd.* **538** (2012) 224–229.

[6] H. Ahlborn, S. Diefenbach, H. Neumann, B. Prinz, L. Ratke, A. Romero: Investigation of the Marangoni-motion on ternary A1-Si-Bi-alloys under microgravity conditions, *Mater. Sci. Eng. A* **173** (1993) 133–135.

[7] A. Munitz, M. Bamberger, A. Venkert, P. Landau, R. Abbaschian: Phase selection in supercooled Cu-Nb alloys, *J. Mater. Sci.* **44** (2008) 64–73.

[8] D. Li, M. Robinson, T. Rathz, G. Williams: Direct determination of the metastable liquid miscibility gap in undercooled Cu–Co alloys, *Mater. Lett.* **36** (1998) 152–156.

[9] Z. Sun, Y. Wang, G. Juan: Liquid phase separation of Cu-Cr alloys during rapid cooling, *Trans. Nonferrous Met. Soc. China (English Ed.)* **16** (2006) 998–1002.

[10] J. Gao, Y. Wang, Z. Zhou, M. Kolbe: Phase separation in undercooled Cu–Cr melts, *Mater. Sci. Eng. A.* **449–451** (2007) 654–657.

[11] Y. Nakagawa: Liquid immiscibility in copper-iron and copper-cobalt systems in the supercooled state, *Acta Metall.* **6** (1958) 704–711.

[12] C. Cao, G. Görler, D. Herlach, B. Wei: Liquid–liquid phase separation in undercooled Co–Cu alloys, *Mater. Sci. Eng. A* **325** (2002) 503–510.

[13] R.P. Shi, C.P. Wang, D. Wheeler, X.J. Liu, Y. Wang: Formation mechanisms of self-organized core/shell and core/shell/corona microstructures in liquid droplets of immiscible alloys, *Acta Mater.* **61** (2013) 1229–1243.

[14] R. Dai, S. Zhang, X. Guo, J. Li: Formation of core-type microstructure in Al–Bi monotectic alloys, *Mater. Lett.* **65** (2011) 322–325.

[15] N. Wang, L. Zhang, Y.L. Peng, W.J. Yao: Composition-dependence of core-shell microstructure formation in monotectic alloys under reduced gravity conditions, *J. Alloys Compd.* **663** (2016) 379–386.

[16] O.E. Jegede, A.M. Mullis, R.F. Cochrane: Metastable monotectic phase separation in Co – Cu alloys, *J. Mater. Sci.* **53** (2018) 11749-11764.

[17] R. Dai, J.F. Zhang, S.G. Zhang, J.G. Li: Liquid immiscibility and core-shell morphology formation in ternary Al-Bi-Sn alloys, *Mater. Charact.* **81** (2013) 49–55.

[18] B. Ma, J. Li, Z. Peng, G. Zhang: Structural morphologies of Cu-Sn-Bi immiscible alloys with varied compositions, *J. Alloys Compd.* **535** (2012) 95–101.

[19] I. Yamauchi, N. Ueno, M. Shimaoka, I. Ohnaka: Undercooling in Co – Cu alloys and its effect on solidification structure, *J. Mater. Sci.* **33** (1998) 371–378.

[20] M. Palumbo, S. Curiotto, L. Battezzati, Thermodynamic analysis of the stable and metastable Co–Cu and Co–Cu–Fe phase diagrams, *Calphad.* **30** (2006) 171–178.

[21] T. Nishizawa, K. Ishida K: The Co–Cu (cobalt–copper) system. *Bull Alloy Phase Diagr.* **5** (1984) 161–165.

[22] O.R. Oloyede, R.F. Cochrane, A.M. Mullis, Effect of rapid solidification on the microstructure and microhardness of BS1452 grade 250 hypoeutectic grey cast iron, *J. Alloys Compd.* **707** (2017) 347-350.

[23] A.M. Mullis, O. Jedge, R.F.Cochrane, Reduced gravity processing of Cu-Co metastable monotectic alloy via drop-tube processing, in: *Proceedings of the 7th International Conference on Solidification & Gravity 2018*, (Eds. A Roosz, Zs Veres, M Sveda & G Karacs), 3-6 September 2018, Miskolc-Lillafüred, Hungary, pp 307-312, Hungarian Academy of Sciences, ISBN 978-963-508-889-8.

[24] I. Kaban, M. Kohler, L. Ratke, W. Hoyer, N. Mattern, J. Eckert, A.L. Greer, Interfacial tension, wetting and nucleation in Al-Bi and Al-Pb monotectic alloys, *Acta Mater*. **59** (2011) 6880–6889.

[25] E.-S. Lee, S. Ahn, Solidification progress and heat transfer analysis of gas-atomizer alloy droplets during spray forming, *Acta Metall. Mater.* **42** (1994) 3231–3143.

[26] N. Wang, B.-B. Wei, Droplet undercooling during containerless processing in a drop-tube, *Chin. Phys. Lett.* **21** (2004) 1120–1123.